Timing jitter of ultrashort solitons in high-speed communication systems. II. Control of jitter by periodic optical phase conjugation

René-Jean Essiambre* and Govind P. Agrawal†

The Institute of Optics and Rochester Theory Center for Optical Science and Engineering, University of Rochester, Rochester, New York, 14627

Received March 5, 1996; revised manuscript received July 17, 1996

We consider the use of periodic optical phase conjugation for reducing the timing jitter in high-speed fiber-optic communication systems employing ultrashort solitons (width < 10 ps) in dispersion-decreasing fibers. Using adiabatic perturbation theory, we derive analytically an expression for the trajectory of a periodically conjugated ultrashort soliton in a communication link after including the effect of amplifier noise and use it to derive the timing jitter in the soliton arrival time at the end of a transmission line. The analysis takes into account not only the group-velocity dispersion but also the Raman effect and the third-order dispersion. We show that the timing jitter can be minimized by using an optimized amplifier spacing ($\sim$65–80 km) for a specific value of average fiber dispersion. The use of shorter amplifier spacings increases timing jitter because of third-order dispersion while for larger amplifier spacings the increased jitter originates from the Raman effect. For high-bit rate systems considered in this paper the Gordon–Haus contribution to the timing jitter is negligible. Under optimized conditions, nearly error-free transmission can be realized at a bit rate of $\sim$100 Gb/s over a distance of 1200 km even in the absence of optical filters. We discuss the role of optical filters for improving system performance and the impact of fiber-dispersion fluctuations on the periodic filtering of ultrashort solitons. © 1997 Optical Society of America [S0740-3224(97)01902-4]

Key words: Amplifier noise, solitons, optical fiber communication, optical phase conjugation, nonlinear optics, optical fiber dispersion.

1. INTRODUCTION

The use of ultrashort solitons (width $<$10 ps) in designing high-speed fiber-optic communication systems (bit rate $>$20 Gb/s) is bringing new challenges for system and fiber designs. In particular, the physical properties of fibers such as optical loss, third-order dispersion (TOD), and the Raman effect, which affect only slightly the dynamics of average solitons (width $>$10 ps), become increasingly of concern for ultrashort soliton propagation.[1] For instance, fiber loss leads to a rapid increase in the emission of dispersive waves as the soliton width decreases. To preserve the nearly ideal properties of solitons over multiple soliton-periods, fibers whose group-velocity dispersion (GVD) decreases with length at the same rate as the soliton energy have been proposed.[2] Such dispersion-decreasing fibers (DDF) can support stable propagation of ultrashort solitons. However, soliton propagation is greatly affected by higher-order effects such as the Raman effect and TOD and may require dispersion tailoring to ensure stable soliton propagation.[3]

An important consequence of higher-order effects on soliton propagation that has attracted relatively little attention is their effect on the transit time of a soliton through a transmission line. In Part I of this paper we derived a general expression [Eq. (I.29); equations of Part I are referred to here by adding a prefactor I] for the timing jitter of ultrashort solitons by including not only the effect of GVD but also the effects of TOD and the Raman effect. Even though emphasis was placed on DDF's simply because such fibers can support ultrashort solitons, the analysis also applies to constant-dispersion fibers provided the amplifier spacing stays much smaller than the soliton period. The results of Part I show that the transmission distance is limited to a few hundreds of kilometers at bit rates of $\sim$100 Gb/s because of the Raman-induced timing jitter. Moreover, in the absence of soliton control the achievable bit rate may be limited to lower values because of soliton interaction.

To extend the transmission distance for long-haul applications, some form of soliton control appears to be necessary. In this paper we consider the use of periodic optical phase conjugation (OPC) for reducing the timing jitter in a soliton communication link made of multiple sections, each containing an optical phase conjugator, an amplifier, and a DDF (see Fig. 1). Previous work[4,5] on the OPC-induced jitter reduction using OPC considers only the effect of GVD and is inherently limited to the average-soliton regime. However, both the Raman effect and TOD add additional fluctuations to the soliton arrival time induced by spontaneous-emission noise of in-line amplifiers. Our analysis shows that not only the Raman and TOD effects are important in the calculation of the timing jitter but also that neglecting such effects may lead to wrong conclusions.

The use of OPC is also advantageous for improving the performance of high-speed communication systems employing ultrashort solitons. For instance, as soliton width decreases toward 1 ps, the frequency downshift due to the Raman effect (soliton self-frequency shift) accumulates rapidly from section to section (see Fig. 1). This fre-

0740-3224/97/020323-08$10.00

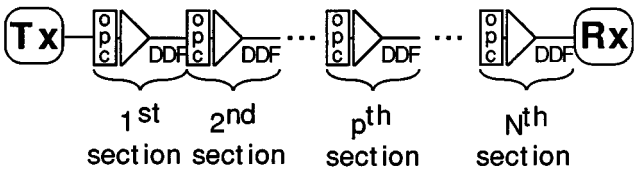

Fig. 1. Schematic representation of a transmission line with periodic amplification and optical phase conjugation. Tx, transmitter; Rx, receiver; OPC, optical phase conjugation; DDF, dispersion-decreasing fiber.

quency shift eventually destroys the soliton after several sections because of the change of GVD with frequency (TOD). It has been shown[6] that the Raman-induced frequency shift occurring over one section can be compensated over a second identical section if the soliton undergoes OPC between the two sections and if fiber loss is neglected. In the presence of fiber loss, Raman compensation is limited to small frequency shifts in the case of constant-dispersion fibers. However, when DDF's are used, a perfect Raman compensation can be achieved because a perfect balance between the GVD and the Kerr nonlinearity is maintained throughout the DDF. A second benefit of OPC is the reversal of soliton interaction.[7,8] In the case of average solitons the reversing of soliton interaction is limited to weak interaction[7,9] because for average solitons the balance between GVD and Kerr nonlinearity is realized only on average.[10] However, the reversing of soliton interactions becomes exact when DDF's are used. Consequently, solitons can be packed together more closely if DDF's are used in place of constant-dispersion fibers. It is important to note that OPC does not compensate for the effects of TOD. Therefore in a soliton communication link employing OPC one may expect an increase in the relative contribution of TOD to the timing jitter compared with the GVD and Raman contributions. Indeed, in contrast with the results of Part I in which the contribution of TOD to the timing jitter is relatively small, TOD becomes the main source of timing jitter for short amplifier spacings when periodic OPC is used.

2. CALCULATION OF THE TIMING JITTER

The most commonly used OPC technique employs nondegenerate four-wave mixing in dispersion-shifted fibers[11–14] chosen such that the GVD parameter β_2 is close to zero at the pump frequency. In the presence of the Raman-induced frequency shift there exists two ways of choosing the pump frequency for the phase conjugator. If the Raman shift is relatively small, the OPC pump frequency may be conveniently set to the soliton input frequency [Fig. 2(a)]. For large Raman frequency shifts such that dispersion tailoring of the DDF becomes necessary,[3] the second fiber segment in each set of two amplification stages would need to have its dispersion tailored differently from the first fiber segment if the OPC pump frequency is chosen as in Fig. 2(a). However, the same fiber design could be used for all segments if the pump frequency of the conjugator is set midway between the input and output frequencies of the signal [Fig. 2(b)].

To evaluate fluctuations in the soliton arrival time at the end of a transmission line (timing jitter), we use the formalism developed in Part I with the conjugator configuration of Fig. 2(a). However, the analysis can be easily extended to the configuration of Fig. 2(b), as discussed in Appendix A. Equation (I.21), established in Part I for the soliton trajectory is also valid for an isolated section of a transmission line shown in Fig. 1. However, the soliton trajectory for a chain of sections with periodic OPC's becomes considerably different. In the following we assume that an OPC is performed before every amplification, as depicted in Fig. 1.

In the notation of Part I a soliton at the end of a section and before entering the phase conjugator can be written as

$$u_s(A,q,\phi,\omega;\tau) = A\ \mathrm{sech}[A(\tau - q)]\exp(i\phi - i\omega\tau), \quad (1)$$

where the amplitude A, position q, phase ϕ, and frequency ω are the normalized soliton parameters. In real units the soliton trajectory becomes $(\omega + \omega_o)T_o$, where ω_o is the carrier frequency and T_o is the soliton width. This soliton is transformed by the phase conjugator into

$$u_s^{\mathrm{conj}}(A,q,\phi,\omega;\tau) = \sqrt{\eta}A\ \mathrm{sech}[A(\tau - q)] \times \exp[-i\phi - i(2\omega_{\mathrm{pump}} - \omega)\tau], \quad (2)$$

where η is the OPC efficiency and ω_{pump} is the frequency of the conjugator pump. Since the conjugator pump frequency is identical to the input soliton frequency in the scheme of Fig. 2(a), $\omega_{\mathrm{pump}} = 0$. The net effect of the OPC is thus to produce a periodic inversion of both the soliton frequency ω and the phase ϕ. As discussed in Part I, the soliton trajectory and the timing jitter of well-isolated solitons are independent of the soliton phase. Since soliton interaction is ignored here, the phase ϕ plays no role in the following analysis.

Since the soliton frequency alternates at each OPC, even- and odd-numbered sections must be treated separately. However, one can take advantage of spectral inversion for canceling displacements over each pair of sections by treating each pair together. Using such a pair of sections as a unit cell, an expression for the soliton dis-

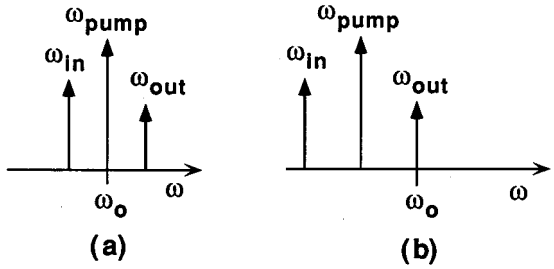

Fig. 2. Two schemes for implementing OPC through the four-wave mixing process: (a) OPC pump frequency ω_{pump} and soliton frequency ω_o (at the input of the link) coincide; (b) ω_{pump} is set midway between ω_o and the frequency ω_{in} of the signal entering the phase conjugator. In a transmission line the frequency at the OPC's output (and at the input of the following fiber) alternates between ω_o and ω_{out} for the scheme of Fig. 2(a) while its stays constant at ω_o for all sections in the case of Fig. 2(b).

placement $\delta q_N^{\rm opc}$ at the end of the transmission line of Fig. 1 is derived in Appendix A. The result is given by

$$\delta q_N^{\rm opc} = q_{\rm GH} \sum_{\substack{p=2\\ p({\rm even})}}^{N} \delta\omega_p + 4(q_R + 2q_{S2}A_{\rm o}^4)A_{\rm o}^3 \sum_{\substack{p=2\\ p({\rm even})}}^{N} \delta A_p + 8q_{S3}A_{\rm o}^7 \sum_{\substack{p=2\\ p({\rm even})}}^{N} \sum_{\substack{i=1\\ i({\rm odd})}}^{p-1} \delta A_i + 16q_{S2}A_{\rm o}^7 \times \sum_{\substack{p=2\\ p({\rm even})}}^{N} \sum_{i=1}^{p-1} \delta A_i + 2q_{\rm TOD}^A A_{\rm o} \sum_{p=1}^{N} \sum_{i=1}^{p} \delta A_i + 2q_{S4}A_{\rm o}^4 \sum_{\substack{p=2\\ p({\rm even})}}^{N} \sum_{\substack{i=2\\ i({\rm even})}}^{p} \delta\omega_i - 2q_{S4}A_{\rm o}^4 \sum_{\substack{p=2\\ p({\rm even})}}^{N} \sum_{\substack{i=1\\ i({\rm odd})}}^{p-1} \delta\omega_i + \sum_{p=1}^{N} \delta q_p , \tag{3}$$

where, to facilitate calculations, the total number N of amplifiers is assumed to be even. The parameters q_{S1}, q_{S2}, q_{S3}, and q_{S4} are defined by Eq. (10) in Appendix A. The average displacement is zero and the root-mean-square (rms) timing jitter $\sigma_q^{\rm opc} \equiv \langle [\delta q_N^{\rm opc}]^2 \rangle^{1/2}$ is given by

$$(\sigma_q^{\rm opc})^2 = \left(\frac{N}{2} q_{\rm GH}^2 + \frac{N^2}{2} q_{\rm GH} q_{S4} A_{\rm o}^4 + \frac{N^3}{3} q_{S4}^2 A_{\rm o}^8 \right) \sigma_\omega^2 + \{4(q_R + 2q_{S2}A_{\rm o}^4)A_{\rm o}^4[2N(q_R + 2q_{S2}A_{\rm o}^4)A_{\rm o}^2 + 4N^2 q_{S2}A_{\rm o}^6 + N^2 q_{\rm TOD}^A] + \frac{8}{3} N^3 A_{\rm o}^{14}(q_{S3}^2 + 4q_{S3}q_{S2} + 8q_{S2}^2) + \frac{8}{3} N^3 (q_{S3} + 4q_{S2}) \times q_{\rm TOD}^A A_{\rm o}^8 + \frac{4}{3} N^3 (q_{\rm TOD}^A)^2 A_{\rm o}^2]\} \sigma_A^2 + N\sigma_q^2, \tag{4}$$

where fluctuations in different soliton parameters and for different amplifiers are assumed to be uncorrelated. In obtaining Eq. (4), summations were replaced by integrals by assuming $N \gg 1$. This expression for $\sigma_q^{\rm opc}$, when compared with σ_q [Eq. (I.29)] of Part I obtained without OPC, shows a substantial reduction of the Raman and Gordon–Haus contributions to the timing jitter mainly because they increase more slowly with an increase in N. This is expected since OPC compensates for both the Raman effect[6] and the effect of GVD.[11] The only term not affected by OPC is the one coming exclusively from TOD [the term involving $(q_{\rm TOD}^A)^2$]. The cross terms (Raman–TOD and GVD–TOD) are, nonetheless, affected by the OPC because frequency conversions are involved in both cases.

3. TIMING JITTER WITH PERIODIC OPTICAL PHASE CONJUGATION

In this section we use Eq. (4) to analyze the timing jitter for different system parameters and discuss the conditions under which the jitter can be minimized. The values of fibers parameters are the same as those used in Part I: TOD coefficient $\beta_3 = 0.07$ ps^3/km and Raman characteristic time $T_R = 6$ fs. We initially set the phase-conjugator efficiency η to 1. The meaning and values of other parameters are discussed in Section 4 of Part I. The parameter N in Eq. (4) is replaced by L/L_A, where L is the total transmission distance and L_A is the amplifier spacing. Since $N \gg 1$, L must exceed a few amplifier spacings for the results to be valid.

The timing jitter for transmission over 2000 km at bit rates in the range 20–100 Gb/s is shown in Fig. 3 by considering several soliton widths in the range 1–10 ps. For comparison, the jitter for a 2-ps soliton without OPC is also shown. As expected, the timing jitter increases rapidly as the pulse width decreases because of both the Raman- and TOD-induced jitter. Nevertheless, the timing jitter for a 2-ps soliton propagating over 1200 km is still relatively low (1.75 ps), allowing nearly error-free transmission at a bit rate of ~100 Gb/s for such a transmission scheme.

By contrast, without OPC, timing jitter of a 2-ps soliton is 1.75 ps after transmission over only ~250 km and becomes 310 ps after 1200 km. In this example, timing jitter is reduced by a factor of 180 at a distance of 1200 km by use of periodic OPC. Moreover, as mentioned before, the use of periodic OPC allows a tighter soliton packing since it helps to reduce soliton interaction.[3] The timing jitter of a 1-ps soliton is relatively high even with the use of periodic OPC. In this case it is the Raman-induced jitter that contributes the most to the timing jitter. For 5- or 10-ps solitons the timing jitter stays relatively low, indicating that such systems can operate over transoceanic distances of ~5000 km.

To illustrate how the relative contributions of various physical effects (GVD, TOD, and Raman effect) are modified with OPC, we plot in Fig. 4 different contributions to the timing jitter as a function of amplifier spacing for a 2-ps soliton bit stream transmitted over 1000 km in DDF's for two values of $\beta_2^{\rm min}$, -0.1 ps^2/km and -0.2 ps^2/km. The solid curve shows the total jitter while other curves represent the partial contributions to the jitter.

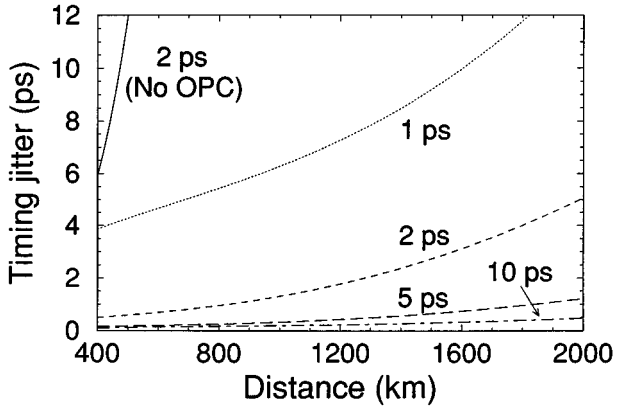

Fig. 3. Timing jitter as a function of transmission distance for four different soliton widths by use of $\beta_2^{\rm min} = -0.3$ ps^2/km and amplifier spacing $L_A = 70$ km. Other parameters are given in the text. For comparison, timing jitter for a 2-ps soliton without OPC is also shown.

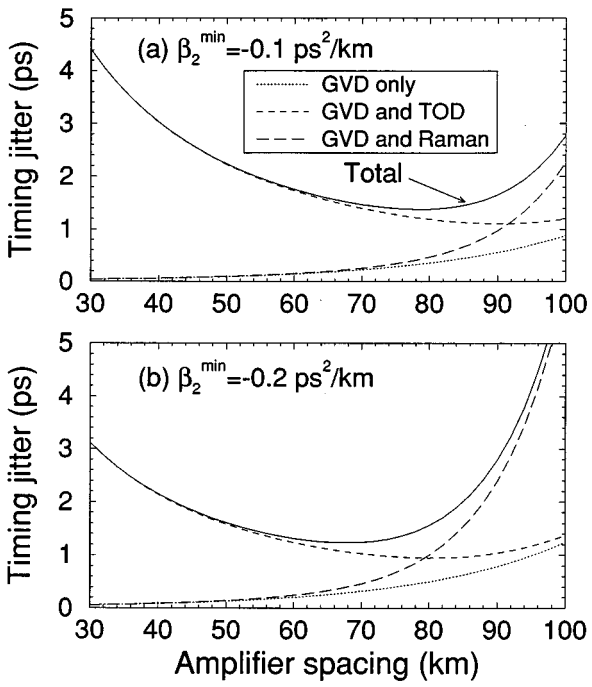

Fig. 4. Timing jitter as a function of amplifier spacing after transmission of 2-ps solitons over 1000 km for DDF's with (a) $\beta_2^{\min} = -0.1$ ps^2/km and (b) $\beta_2^{\min} = -0.2$ ps^2/km. In both cases an optimum amplifier spacing can be used to minimize timing jitter.

When GVD is the sole mechanism generating the timing jitter (dotted curves in Fig. 4), we recover the Gordon–Haus jitter for a system with OPC. This curve represents the timing jitter that would be predicted if the analyses of Refs. 4, 5, and 9 were directly applied to the scheme of Fig. 1. As Fig. 4 shows clearly, such a description is incomplete and cannot predict accurately the value of the timing jitter in a system with periodic OPC simply because higher-order effects are completely neglected. In fact, the Gordon–Haus contribution to the jitter becomes practically negligible as a result of the OPC-induced compensation of the GVD effects. For moderate amplifier spacings [<85 km in Fig. 4(a) and <70 km in Fig. 4(b)] the timing jitter is almost exclusively due to TOD because of the overall low average GVD and the N^3 dependence in Eq. (4) for TOD. For large amplifier spacings the Gordon–Haus jitter increases but is overwhelmed by the Raman-induced timing jitter, which increases more rapidly with L_A. In that case it is the relatively high average dispersion (large amplifier spacings require high values of $|\beta_2^{\max}|$, $\beta_2^{\max}$ being the GVD at the input end) that is responsible for this transition from the β_3 dominance to the Raman dominance as the amplifier spacing increases beyond a certain value. From a practical standpoint, Fig. 4 shows clearly that, for a given set of fiber and soliton parameters, timing jitter can be minimized by choosing an optimum value of amplifier spacing, typically in the range of 60–90 km. Such optimized amplifier spacings have not been predicted so far because, to our knowledge, it is the first time that both the Raman- and third-order dispersion-induced contributions are included in the calculation of the timing jitter in a communication system with OPC. It is interesting to note that the main result of using a fiber with a high value of $|\beta_2^{\min}|$ is to downshift the timing-jitter minimum toward smaller amplifier spacings in such a way that the maximum value $\beta_2^{\max}$ of GVD at the fiber input remains nearly the same.

To better characterize the origin of timing jitter, we plot in Fig. 5 the relative contributions of amplitude and frequency fluctuations under operating conditions identical to those of Fig. 4(b). Clearly, amplitude fluctuations are the main source of timing jitter for all practical amplifier spacings. The influence of frequency fluctuations on the jitter (Gordon–Haus component) is small and results in an increase of the total timing jitter by less than 5%. Figure 5 suggests that a precise control of the soliton amplitude is the key in reducing the timing jitter.

As seen in Figs. 4 and 5, an optimum amplifier spacing exists that minimizes the timing jitter for a given DDF. However, this optimum amplifier spacing depends on the minimum and maximum values of GVD occurring in the DDF. To represent this dependence, Fig. 6 shows a contour plot of the timing jitter in the L_A–$\beta_2^{\min}$ plane for 2-ps solitons over 1000 km. The innermost contour encloses the parameter region for which the timing jitter is less than 1.1 ps; timing jitter increases by 0.1 ps for each subsequent contour. Nearly error-free operation at bit rates $B \sim 100$ Gb/s requires the timing jitter to be below approximately $0.164/B = 1.64$ ps. The corresponding parameter space is bounded by the sixth contour. Figure 6 also shows that low values of $|\beta_2^{\min}|$ are also preferable and allow for a larger amplifier spacing. Regions where $|\beta_2^{\min}| < 0.1$ ps^2/km are not displayed in Fig. 6 since increasing emission of dispersive waves may occur for such values of $\beta_2^{\min}$.

Phase conjugation can be a process of limited efficiency.[12] Low efficiencies must be compensated by use of higher amplifier gains. To evaluate the impact of phase-conjugation efficiencies on the timing jitter, we replace the amplifier gain G in Eqs. (I.30) by $G = \exp(\alpha z_a)/\eta$, where the efficiency η is the fraction of energy contained in the conjugate signal. Figure 7 shows how jitter increases with a decrease in the efficiency over a range of 10 dB. The increase in the timing jitter as the conversion efficiency decreases comes from the supplementary noise introduced by the additional gain neces-

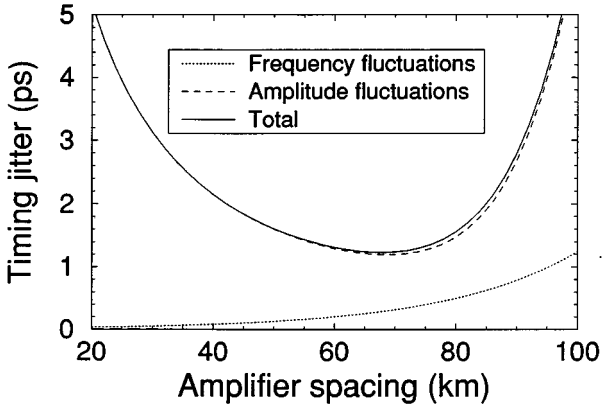

Fig. 5. Contribution of amplitude and frequency fluctuations to the total timing jitter for the case of Fig. 2(b). Amplitude fluctuations dominate the jitter for all amplifier spacing when 2-ps solitons are transmitted over 1000 km.

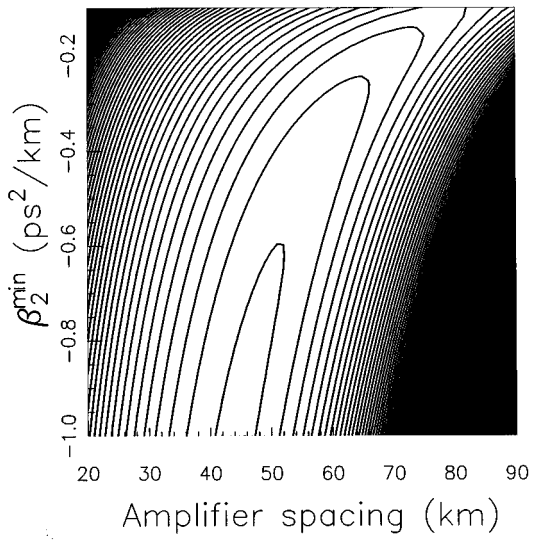

Fig. 6. Contour plot of the timing jitter as a function of amplifier spacing L_A and $\beta_2^{\min}$ for 2-ps solitons transmitted over 1000 km. The innermost contour encloses a region of timing jitter less than 1.1 ps. The timing jitter increases by 0.1 ps for each successive contour.

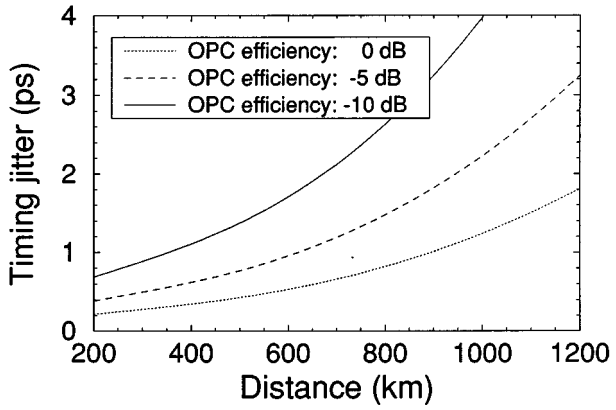

Fig. 7. Effect of phase-conjugator efficiency on the timing jitter for $T_s = 2$ ps, $\beta_2^{\min} = -0.2$ ps^2/km, and amplifier spacing $L_A = 70$ km. Jitter increases for lower efficiencies because of the additional gain needed to compensate for the low efficiencies.

sary to compensate for the low efficiency of phase conjugators. For a −5-dB efficiency (32% conversion) the timing jitter of a 2-ps soliton is ~2 ps after 1000 km. For a lower efficiency of −10 dB (10% conversion into the conjugate signal) the same timing jitter occurs after a distance of only 680 km. The use of a conjugator with low efficiencies will thus shorten the transmission distance or require some additional form of control. It has recently been shown[13] that efficiencies as high as −4.6 dB could be achieved when a fiber is used for OPC if the pump is modulated to suppress stimulated Brillouin scattering. Furthermore, efficiencies in excess of 0 dB are predicted[14] if the nonlinear detuning of phase matching is compensated by tuning the OPC pump frequency in the anomalous dispersion region of the OPC fiber. However, since OPC operation at high conversion efficiencies generally requires relatively long fiber lengths, dispersion within the OPC fiber itself may broaden the conjugate soliton. One may reduce this soliton broadening by using a shorter fiber length (at the expense of the conversion efficiency), or one may use some form of dispersion compensation at the output of the OPC fiber.

To further reduce the timing jitter, insertion of bandpass filters may be of practical interest. It is interesting to note here that the use of sliding filters[15] does not appear to be necessary since the soliton-train spectrum itself shifts by a significant amount between the input and output of each DDF. This Raman-induced frequency shift plays the role that the sliding of the filter frequency played in the sliding-frequency filter technique, thereby allowing the use of filters of fixed central frequency. By filtering the signal before and after each DDF with two fixed-frequencies bandpass filters (centered at the solitons' mean frequencies at the input and output ends, respectively), efficient filtering of the noise can be realized. If the central frequencies of the two filters (determined by the Raman frequency shift) are sufficiently far apart, amplifier noise will be drastically cut while solitons pass through the two filters with little attenuation. Since Raman shifts can be quite large for ultrashort solitons, very efficient filtering of the noise can be achieved over the entire spectrum after few amplifier spacings because the soliton frequency shift can be greater than the filter bandwidth. Moreover, insertion of bandpass filters should result in considerable damping of both amplitude and frequency fluctuations, resulting in further reduction of the timing jitter. However, a nonideal dispersion profile of the DDF's is likely to modify the Raman shift and may reduce the effectiveness of the use of bandpass filters. Section 4 considers the effects of dispersion variations on the Raman-induced frequency shift.

4. EFFECT OF NONIDEAL DISPERSION PROFILES

In Section 3 we considered an ideal dispersion profile, matching losses (and other higher-order effects for ultrashort solitons). However, variations from the ideal dispersion profile may occur because of fabrication constraints. Clearly, if these variations are relatively small and occur at low spatial frequencies, the soliton will adapt adiabatically to the local GVD and change its amplitude, which in turn will modify the soliton trajectory due to the Raman effect. If dispersion variations have large amplitudes or occur at high spatial frequencies such that the length scale of variations is comparable to the local soliton period, nonadiabatic propagation will generally lead to emission of dispersive waves.[16] The role of dispersion variations of spatial periods much shorter than the soliton period is similar to the role of loss-induced energy variations in the average-soliton regime[16,17]: For sufficiently rapid dispersion variations it is the average dispersion that the soliton will experience with minimal generation of dispersive waves.

Fiber-dispersion variations, being fixed once the fiber is drawn, will affect a soliton in different sections in the same way only if all fiber sections were identical. In practice, dispersion variations are likely to vary randomly from fiber to fiber in a cascaded chain of amplifiers. Contribution of such variations to the timing jitter requires a more detailed analysis and is not considered here. In-

stead, we consider the first-order effect of a nonideal dispersion profile such that it produces a different Raman-induced frequency shift than the one expected from the DDF having an ideal dispersion profile. This change in the soliton mean frequency would be of little consequence if optical filters were absent from the system. However, such filters are likely to be present, either to separate the phase-conjugate signal from the pump (in a forward four-wave mixing scheme[12]) or/and to reduce the timing jitter. Since the central frequency of these filters is determined by assuming ideal dispersion profiles during the design process, variations in the dispersion profiles will result in a mismatch between the mean frequency of solitons and the central frequency of bandpass filters. If this mismatch is not small compared with both the soliton and filter bandwidths, a significant loss of soliton energy will occur at the filters, a loss that may eventually result in the destruction of the soliton bit stream. The following calculation provides an estimate of the Raman-induced frequency shift induced by dispersion variations.

Dispersion variations are taken into account by use of $p(z) = \bar{p}(z) + \tilde{p}(z)$ for the dispersion profile, where $\bar{p}(z) = \exp(-\alpha z)$ is for an ideal loss-matched profile and $\tilde{p}(z)$ represents a small variation of the spatial period larger than the soliton period. It is worth stressing that our choice of ideal dispersion profile $\bar{p}(z)$ is not restrictive, and the analysis can also be applied to other custom-tailored dispersion profiles.

For the type of perturbations $\tilde{p}(z)$ considered here, the soliton dynamic is adiabatic. The evolution of the soliton mean frequency $\omega(z)$ is obtained by use of relations (I.15) and (I.16) and is given by

$$\omega(z) = -\frac{8}{15}\,\tau_R A_o^4 z_1(z) + \frac{8}{15}\,\tau_R \times A_o^4\left[3\int_0^z \tilde{p}(z')\mathrm{d}z' - 6\int_0^z \frac{\tilde{p}^2(z')}{\bar{p}(z')}\,\mathrm{d}z'\right], \quad (5)$$

where the first term on the right side is simply the frequency shift occurring in the ideal DDF and the following two terms are the frequency shifts associated with the nonideal nature of the profile. Interestingly, the frequency shift associated with dispersion variations depends not only on the average of dispersions fluctuations [second term of the right side of Eq. (5)] but also includes a weaker second-order term [last term of Eq. (5)]. The latter source of frequency shift arises because the frequency shift due to the Raman effect does not depend linearly on the soliton amplitude. However, this contribution is likely to be much smaller than the one coming from $\int\tilde{p}(z)\mathrm{d}z$ (unless average dispersion variations can be made very small by some fiber-drawing technique), and we neglect it here. To provide an estimate, we use the form

$$\tilde{p}(z) = \frac{\Delta\beta_2}{|\beta_2^{\max}|}\sin\left(\frac{\pi z}{z_a}\right), \quad (6)$$

which is a perturbation having a half-period equal to the length of the DDF's. Here $\Delta\beta_2$ is the amplitude of dispersion variations such that $|\Delta\beta_2| \ll \bar{p}(z)|\beta_2^{\max}|$. A more complete description would consider a sum of sinusoids of different periods and amplitudes (i.e., a Fourier series). Moreover, the exact soliton propagation dynamics under dispersion variations of various spatial frequencies would need to be taken into account.[16] In our model the frequency shift associated with dispersion variations given by Eq. (6) is directly obtained from Eq. (5).

Figure 8 shows the additional soliton frequency shift generated by dispersion variations for several values of soliton widths T_s by normalizing it to the soliton's own bandwidth ($\Delta\nu_s \approx 0.315/T_s$). Solitons broader than 2 ps shift by a very small fraction of their bandwidth for a wide range of dispersion variations. For a 1-ps soliton, dispersion variations become more critical, as they can shift the soliton spectrum by as much as 30% of its spectral width. For 700-fs solitons the sliding of the soliton spectrum becomes comparable with the soliton spectral bandwidth unless dispersion variations are made very small by a precise control of the dispersion profile. In the pioneering work related to the fabrication of DDF's,[18] a precision on $|\beta_2|$ of $\sim$0.12 ps^2/km has been reported. The results shown in Fig. 8 suggest that dispersion fluctuations are not likely to affect the system performance when soliton width exceeds 2 ps but may be detrimental to the system for subpicosecond solitons. Further improvements in the fabrication technique may solve this problem.

Another important point concerning fiber design and fabrication is related to the absolute value of the minimum dispersion $|\beta_2^{\min}|$ achievable at the fiber end. As discussed in Section 2 of Part I, our numerical simulations show that TOD can lead to excessive generation of dispersive waves if $|\beta_2^{\min}|$ becomes too small. This acceptable value of $|\beta_2^{\min}|$ depends on several design parameters but ranges typically between 0.05 and 0.2 ps^2/km. We also numerically observed soliton broadening for low values of $|\beta_2^{\min}|$. One way to prevent this broadening would be to lower the rate of GVD decrease toward the fiber end so that solitons compress slightly and recover their desired amplitude. Another design could take advantage of the fact that the local soliton period toward the fiber end may be approximately 5–20 km. In this case, dispersion profiling can be stopped before the fiber end, GVD can be

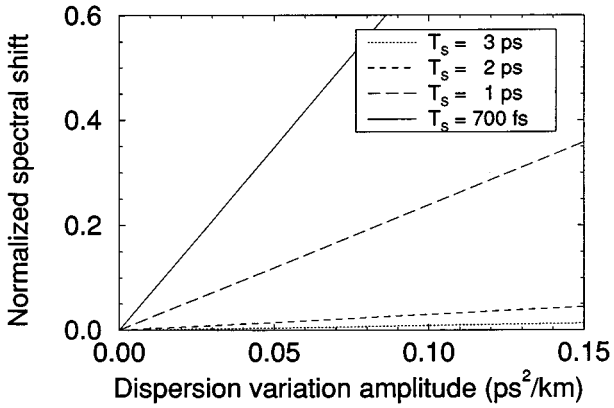

Fig. 8. Spectral shift of a soliton (normalized to its own spectral width) as a function of the amplitude of dispersion variations for several solitons widths. Spectral shifts in excess of 10% may limit the use of bandpass filters for soliton control.

abruptly lowered to the appropriate level of an average soliton, and the last few kilometers of fiber can be drawn at constant dispersion. Moreover, lowering of dispersion may not even be necessary because compensation of soliton broadening (due to TOD) often requires higher GVD. In such a design, dispersion profiling will be stopped a few kilometers before the fiber end, and the GVD will be kept constant to that value for the last few kilometers.

5. CONCLUSION

Using adiabatic perturbation theory, we have derived an expression for the soliton trajectory and timing jitter in a high-speed communication system making use of ultrashort solitons in DDF's and employing the technique of periodic OPC for jitter control. We found that neglecting TOD and the Raman effect results in an underestimate of timing jitter and that inclusion of these effects shows the existence of an optimum amplifier spacing (65–80 km) that minimizes the timing jitter. For shorter amplifier spacings the increase of the timing jitter originates in the third-order dispersion, while for large amplifier spacings it is the Raman effect that increases the jitter. We also found that the timing jitter originates mostly from amplitude fluctuations imposed on solitons during their amplification by the spontaneous-emission noise. If one considers only the jitter from fiber dispersion and higher-order effects as in this paper, the use of optical phase conjugation can reduce sufficiently the timing jitter to allow nearly error-free transmission at bit rates of ~100 Gb/s over ~1200 km without optical filters. Optical filters should increase the transmission distance considerably. The constraints imposed by fiber dispersion variations of various amplitude on the use of optical filters with ultrashort solitons have been estimated. Variations from the ideal dispersion profile of the fiber may ultimately determine the minimum soliton width and consequently set a maximum bit rate at which long-haul subpicosecond solitons-based communications systems can operate.

APPENDIX A: SOLITON TRAJECTORY IN THE PRESENCE OF FLUCTUATIONS IN A PERIODICALLY PHASE-CONJUGATED SYSTEM

In this appendix we derive an expression [Eq. (3)] for the soliton timing jitter $\delta q_N^{\rm opc}$ for the communication system of Fig. 1. We proceed as in the appendix of Part I and start with the evolution equations for the soliton parameters [Eqs. (I.31)–(I.33)]. We focus on the case of Fig. 2(a), where the pump frequency coincides with the soliton input frequency.

Since OPC does not affect amplitude fluctuations, Eq. (I.35) can be used as such. However, the evolution of the soliton frequency $\omega_p^{\rm opc}(z)$ in the pth section is quite different than Eq. (I.37) when OPC is included. It becomes necessary to consider even- and odd-numbered sections separately since the unit cell now contains a pair of two neighboring sections (see Fig. 9). By taking into account

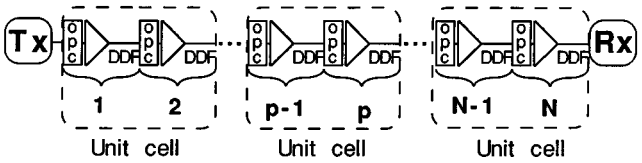

Fig. 9. Schematic of the unit cell used for calculating soliton displacement $q_N^{\rm opc}$.

an OPC-induced spectral inversion, the soliton frequency evolution for even-numbered and odd-numbered sections can be written as

$$\omega_p^{\rm opc}(z) = \frac{8}{15}\tau_R z_1(z_a)A_{\rm o}^4 - \frac{8}{15}\tau_R z_1(z)A_{\rm o}^4 + \frac{32}{15}\tau_R z_1(z_a)A_{\rm o}^3\sum_{\substack{i=1\\ i({\rm odd})}}^{p-1}\delta A_i - \frac{32}{15}\tau_R z_1(z) \times A_{\rm o}^3\sum_{i=1}^{p}\delta A_i - \sum_{\substack{i=1\\ i({\rm odd})}}^{p-1}\delta\omega_i + \sum_{\substack{i=2\\ i({\rm even})}}^{p}\delta\omega_i, \quad (7)$$

$$\omega_{p-1}^{\rm opc}(z) = -\frac{8}{15}\tau_R z_1(z)A_{\rm o}^4 + \frac{32}{15}\tau_R z_1(z_a)A_{\rm o}^3\sum_{\substack{i=2\\ i({\rm even})}}^{p-2}\delta A_i - \frac{32}{15}\tau_R z_1(z)A_{\rm o}^3\sum_{i=1}^{p-1}\delta A_i + \sum_{\substack{i=1\\ i({\rm odd})}}^{p-1}\delta\omega_i - \sum_{\substack{i=2\\ i({\rm even})}}^{p-2}\delta\omega_i. \quad (8)$$

These equations are used in Eq. (I.33) for calculating the soliton trajectories for the pth and the $(p-1)$th sections separately. The resulting soliton displacements are $q_p^{\rm opc}(z_a)$ and $q_{p-1}^{\rm opc}(z_a)$, respectively. The two displacements are summed to obtain the total displacement for a unit cell. In doing so, many terms cancel out. After a tedious but straightforward calculation, we obtain the following recurrence relation:

$$q_p^{\rm opc}(z_a) = 2q_{\rm TOD}^A A_{\rm o}^2 + 2q_{\rm S1}A_{\rm o}^8 + q_{\rm GH}\delta\omega_p + 4(q_R + 2q_{\rm S2}A_{\rm o}^4)A_{\rm o}^3\delta A_p + 8q_{\rm S3} \times A_{\rm o}^7\sum_{\substack{i=1\\ i({\rm odd})}}^{p-1}\delta A_i + 16q_{\rm S2}A_{\rm o}^7\sum_{i=1}^{p-1}\delta A_i + 2q_{\rm TOD}^A \times A_{\rm o}\left(\sum_{i=1}^{p}\delta A_i + \sum_{i=1}^{p-1}\delta A_i\right) + 2q_{\rm S4}A_{\rm o}^4\left(\sum_{\substack{i=2\\ i({\rm even})}}^{p}\delta\omega_i - \sum_{\substack{i=1\\ i({\rm odd})}}^{p-1}\delta\omega_i\right) + \delta q_p + \delta q_{p-1} + q_{p-2}^{\rm opc}(z_a), \quad (9)$$

where we defined the following four parameters:

$$q_{S1} = \frac{64}{75}\frac{\delta_d \tau_R^2}{\alpha^2}(z_a - \alpha z_a z_2 - z_2), \quad q_{S3} = \frac{64}{75}\delta_d \tau_R^2 z_a z_1^2,$$

$$q_{S2} = \frac{64}{75}\frac{\delta_d \tau_R^2}{\alpha^2}(z_a - \alpha z_a z_1 - z_2), \quad q_{S4} = \frac{8}{5}\delta_d \tau_R z_a z_1. \tag{10}$$

We adopt the convention that all q functions are evaluated at $z = z_a$ when the z dependence is not shown explicitly. By solving the recurrence relation (9) for a chain of N amplifiers (N even), we obtain the soliton displacement

$$\begin{aligned} q_N^{\mathrm{opc}} = {} & q_{\mathrm{TOD}}^A \sum_{p=1}^{N} A_o^2 + q_{S1} \sum_{p=1}^{N} A_o^8 + q_{GH} \sum_{\substack{p=2 \\ p(\mathrm{even})}}^{N} \delta\omega_p \\ & + 4(q_R + 2q_{S2}A_o^4)A_o^3 \sum_{\substack{p=2 \\ p(\mathrm{even})}}^{N} \delta A_p + 8q_{S3} \\ & \times A_o^7 \sum_{\substack{p=2 \\ p(\mathrm{even})}}^{N} \sum_{\substack{i=1 \\ i(\mathrm{odd})}}^{p-1} \delta A_i + 16q_{S2}A_o^7 \sum_{\substack{p=2 \\ p(\mathrm{even})}}^{N} \sum_{i=1}^{p-1} \delta A_i \\ & + 2q_{\mathrm{TOD}}^A A_o \sum_{p=1}^{N} \sum_{i=1}^{p} \delta A_i + 2q_{S4}A_o^4 \sum_{\substack{p=2 \\ p(\mathrm{even})}}^{N} \sum_{\substack{i=2 \\ i(\mathrm{even})}}^{p} \delta\omega_i \\ & - 2q_{S4}A_o^4 \sum_{\substack{p=2 \\ p(\mathrm{even})}}^{N} \sum_{\substack{i=1 \\ i(\mathrm{odd})}}^{p-1} \delta\omega_i + \sum_{p=1}^{N} \delta q_p . \end{aligned} \tag{11}$$

The average soliton displacement (in the absence of amplifier noise) is given by the first two terms of Eq. (11). Note that the average displacement is zero when TOD is neglected ($\delta_d = 0$). However, when TOD is taken into account, the Raman effect also contributes to the average displacement through the second term involving q_{S1}.

Timing jitter [Eq. (3) in the main text] $\delta q_N^{\mathrm{opc}}$ is obtained from Eq. (11) by removing the first two terms.

The calculation of soliton trajectory for a system using the scheme of Fig. 2(b) for OPC can be treated by the formulation used here for the OPC configuration of Fig. 2(a). In the case of Fig. 2(b) the form of the frequency evolution is the same for all sections and can be obtained for the pth section from Eq. (8) by replacing p by $p + 1$ and extending all summations over i to all integer values.

ACKNOWLEDGMENTS

This work was supported by the Fonds pour la Formation de Chercheurs et l'Aide à la Recherche of the Québec government (Canada), the U.S. Army Research Office, and the National Science Foundation (grant PHY94-15583)

*E-mail, rjessiam@optics.rochester.edu; telephone, 716 275-6892; fax, 716 244-4936.

†E-mail, gpa@optics.rochester.edu; telephone, 716 275-4846; fax; 716 244-4936.

REFERENCES

1. G. P. Agrawal, *Nonlinear Fiber Optics*, 2nd ed. (Academic, Boston, Mass., 1995).
2. K. Tajima, "Compensation of soliton broadening in nonlinear optical fibers with loss," Opt. Lett. **12**, 54–56 (1987).
3. R.-J. Essiambre and G. P. Agrawal, "Ultrahigh bit-rate soliton communication systems using dispersion-decreasing fibers and parametric amplifiers," Opt. Lett. **21**, 116–118 (1996).
4. W. Forysiak and N. J. Doran, "Reduction of Gordon–Haus jitter in soliton transmission systems by optical phase conjugation," J. Lightwave Technol. **13**, 850–855 (1995).
5. C. G. Goedde, W. L. Kath, and P. Kumar, "Periodic amplification and conjugation of optical solitons," Opt. Lett. **20**, 1365–1367 (1995).
6. S. Chi and S. Wen, "Recovery of the soliton self-frequency shift by optical phase conjugation," Opt. Lett. **19**, 1705–1707 (1994).
7. W. Forysiak and N. J. Doran "Conjugate solitons in amplified optical fiber transmission systems," Electron. Lett. **30**, 154–155 (1994).
8. S. Wen and S. Chi, "Undoing of soliton interaction by optical phase conjugation," Electron. Lett. **30**, 663–664 (1994).
9. S. Wen and S. Chi, "Reduction of the soliton interaction and the Gordon–Haus effect by optical phase conjugation," Opt. Lett. **20**, 976–978 (1995).
10. A. Hasegawa and Y. Kodama "Guiding-center soliton in optical fibers," Opt. Lett. **15**, 1443–1445 (1990).
11. A. Yariv, D. Fekete, and D. M. Pepper, "Compensation for channel dispersion by nonlinear optical phase conjugation," Opt. Lett. **4**, 52–54 (1979).
12. S. Watanabe, T. Chikama, G. Ishikawa, T. Terahara, and H. Kuwahara, "Compensation of pulse shape distortion due to chromatic dispersion and Kerr effect by optical phase conjugation," IEEE Photonics Technol. Lett. **5**, 1241–1243 (1993).
13. S. Watanabe and T. Chikama, "Highly efficient conversion and parametric gain of nondegenerate forward four-wave mixing in a singlemode fibre," Electron. Lett. **30**, 163–164 (1994).
14. S. Wabnitz, "Nonlinear enhancement and optimization of phase-conjugation efficiency in optical fibers," IEEE Photonics Technol. Lett. **7**, 652–654 (1995).
15. L. F. Mollenauer, J. P. Gordon, and S. G. Evangelides, "The sliding-frequency guiding filter: an improved form of soliton control," Opt. Lett. **17**, 1575–1577 (1992).
16. F. K. Abdullaev, J. G. Caputo, and N. Flytzanis, "Envelope soliton propagation in media with temporally modulated dispersion," Phys. Rev. E **50**, 1552–1558 (1994).
17. B. A. Malomed, D. F. Parker, and N. F. Smyth, "Resonant shape oscillations and decay of a soliton in a periodically inhomogeneous nonlinear optical fiber," Phys. Rev. E **48**, 1418–1425 (1993).
18. V. A. Bogatyrev, M. M. Bubnov, E. M. Dianov, A. S. Kurkov, P. V. Mamyshev, A. M. Prokhorov, S. D. Rumyantsev, V. A. Semenov, S. L. Semenov, A. A. Sysoliatin, S. V. Chernikov, A. N. Gur'yanov, G. G. Devyatykh, and S. I. Miroshnichenko, "A single-mode fiber with chromatic dispersion varying along the length," J. Lightwave Technol. **9**, 561–566 (1991).